Electrochemistry Communications 143 (2022) 107391

Contents lists available at ScienceDirect

Electrochemistry Communications

journal homepage: www.elsevier.com/locate/elecom

Short Communication

Features of the porous morphology of anodic alumina films at the initial stage of disordered growth

Katsiaryna Chernyakova [a,*], Vaclovas Klimas [a], Arunas Jagminas [a], Nikita Lushpa [b], Igor Vrublevsky [b], Sigitas Jankauskas [a]

[a] State Research Institute Center for Physical Sciences and Technology, Sauletekio ave. 3, LT-10257 Vilnius, Lithuania
[b] Belarussian State University of Informatics and Radioelectronics, P. Brovki 6, 10213 Minsk, Belarus

ARTICLE INFO

Keywords:
Porous alumina films
Disordered growth
Major pore diameter
Minor pore diameter

ABSTRACT

A characteristic feature of disordered porous anodic film growth at the initial stage of aluminum anodizing was revealed by varying the electrolyte type and anodizing voltage. The samples were obtained by the electrochemical oxidation of thin aluminum films (100 nm thick) on SiO_2/Si substrates in a 0.3 M oxalic acid at 10–50 V and were studied by SEM. The ImageJ analysis of the images revealed the simultaneous development of two large groups of pores: major pores with a large diameter and minor pores with a smaller diameter. When anodizing in oxalic acid at 10–50 V, it has been shown that the ratio of the diameters of the major and minor pores remains constant and is about 1.17. Using a geometric model, we demonstrated that the centers of the minor pores are located inside the elementary hexagonal cell formed by the centers of the major pores. Moreover, our results are very close to the theoretical value of $2/\sqrt{3}$. At the initial stage of disordered pore growth, the development of minor pores rather than major pores is not a random process and is determined by energy-efficient conditions for the development of pores inside the hexagonal cells formed by the major pores. The increase in compressive mechanical stress in the anodic film leads to an interruption in the development of such pores.

1. Introduction

Porous anodic alumina films with nanosized pores are promising materials for applications in catalysis, optics, sensors, and nanotechnologies [1–5]. An important step in forming highly ordered porous structures was the discovery of the two-stage formation of porous alumina [6,7]. This led to a rapid increase in research into the peculiarities of anodic film growth [8–13] and the properties of porous anodic alumina with a given pore geometry [14–17]. It is well known that, immediately after the voltage is applied, the nucleation of pores on the aluminum surface is random. However, the development of major pores with large diameters, with the diameter determined by the anodization voltage, becomes a dominant process [18,19]. If the layer of the primary porous anodic alumina is removed by selective etching on the aluminum surface, the surface texture of the porous oxide structure will remain with the main pores in the form of cavities. During a second anodization of aluminum at the same voltage, the surface texture on the aluminum surface will serve as centers for the nucleation of major pores. Therefore, porous anodic alumina films formed by this method have a highly ordered porous structure [1]. At the same time, it can be assumed that the development of pores at the initial stage of the disordered porous anodic film growth during aluminum anodization has characteristic features. However, such regularities in the initial development of pores have been little studied.

The purpose of this work was therefore to study regularities in the development of porous anodic films at the initial stage of disordered growth at various anodizing voltages.

2. Materials and methods

Thin aluminum films (about 100 nm) were obtained by aluminum deposition on silicon substrates with a thin silicon dioxide film (SiO_2/Si wafers) by thermal evaporation in a vacuum. The SiO_2/Si substrate was chosen due to its high thermal conductivity (149 W m^{-1} K^{-1}), which is slightly less than that of aluminum (200 W m^{-1} K^{-1}). This was also connected to the need for a standard aluminum film thickness in experiments with different anodizing modes. Then, square samples with an area of no more than 7.2 cm^2 were cut from the substrates, and were

* Corresponding author.
E-mail address: katsiaryna.charniakova@ftmc.lt (K. Chernyakova).

https://doi.org/10.1016/j.elecom.2022.107391
Received 11 October 2022; Received in revised form 28 October 2022; Accepted 29 October 2022
Available online 30 October 2022

then immersed in a 0.3 M aqueous solution of oxalic acid and anodized under constant voltage and temperature conditions until the aluminum film was completely anodized. The anodizing voltage (U_a) ranged from 10 to 50 V, and the temperature was 20 °C. The times of through-anodization of the aluminum film for voltages of 10, 15, 20, 30, 40, and 50 V were 7.5, 5, 3.5, 2, 1.8, and 1.0 min, respectively. To compare the surface morphologies of the porous alumina obtained in different electrolytes, one sample was anodized in a 1.8 M aqueous solution of sulfuric acid at a constant voltage of 16 V (anodizing time was about 60 s). An anodizing area equal to 3.14 cm^2 was set by Viton-o-ring. The anodizing process was conducted in a two-electrode fluoroplastic cell, identical to the one described in [12]. A constant current source PI50 1 was used for the anodizing process. The electrolyte temperature was kept constant using a cryostat WK 230 (Lauda). A platinum grid was used as the cathode. The electrolyte was vigorously stirred by a magnetic stirrer.

Additionally, we formed samples on high-purity Al foil (99.999 %, 250 μm, Alfa Aesar) for the two-stage anodizing experiments and experiments on electropolished Al foil to investigate the peculiarities of the initial growth of the porous anodic alumina on bulk samples. The preliminary preparations and the process of two-stage anodizing of the aluminum foil samples are described in [10]. Anodizing was conducted in a 0.3 M aqueous solution of oxalic acid at 20 °C and 50 V for 30 min. Electropolishing was carried out in a $HClO_4$-Eth-glycerol solution at 5 °C and 17 V dc for 5 min.

The surface morphology of the porous anodic alumina films was studied by scanning electron microscopy (SEM) using an electron microscope (Model Quanta 200F electron microscope (FEI)) with further computer processing of images in the ImageJ software following the data processing procedure described in [12]. The determination error d_{pore} did not exceed 3.5 %.

3. Results and discussions

It can be seen from the SEM studies that the aluminum films on the Si/SO_2 substrate were anodized completely, and the final anodic alumina pores were cylindrical and ordered in the direction perpendicular to the substrate surface (Fig. 1). Porous anodic alumina films with a highly ordered structure consist of a close-packed, hexagonally-ordered array of cells with a pore located in the center of each cell. In this case, the pore diameter is proportional to the anodizing voltage. Therefore, it is essential to study thin porous anodic films formed at different anodizing voltages and compare their morphological characteristics. On the surface, the films obtained in 0.3 M oxalic acid at 10–50 V are porous. As shown in Fig. 2, on increasing the anodizing voltage from 10 to 50 V, the pore diameter increases with a simultaneous decrease in their number per unit area.

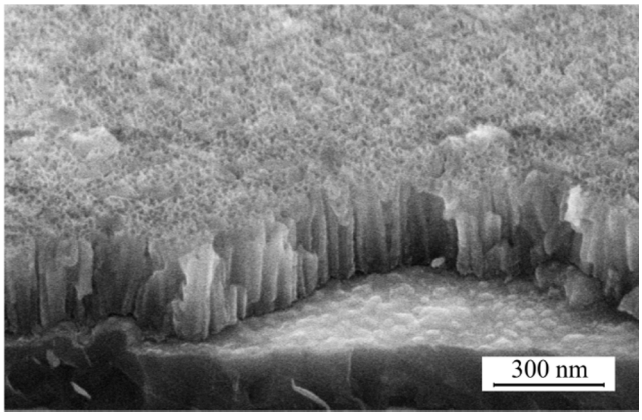

Fig. 1. SEM image of a cross-section of the thin porous anodic alumina film obtained on the Si/SiO_2 substrate.

As can be seen from Fig. 3, the pore distribution by diameter for oxalic acid porous alumina films has two distinct peaks, at about 17.5 and 20.5 nm. This is characteristic of disordered pore growth at the initial stage of aluminum anodizing, when two different groups of pores are developing: pores of a larger diameter (major pores) and pores of a smaller diameter (minor pores).

We also obtained sulfuric acid anodic alumina films to determine if the regularities of disordered anodic films at the initial anodization stage depend on the electrolyte type. From Fig. 3, it can be seen that the pore distribution by diameter also has two peaks, at around 7.3 and 8.6 nm.

To show how the anodizing voltage and electrolyte affect the ratio of the diameters of the major and minor pores, we introduced the coefficient *K,* which is equal to the ratio of the diameter of major pores (D) to the diameter of minor pores (d) (Table 1):

$$K = D/d.$$

Analysis of the data in Table 1 shows that for oxalic acid anodizing in the U_a range 10–50 V, K does not depend on the U_a and is approximately equal to 1.17. K also does not depend on electrolyte type because, for a porous anodic alumina film formed in 1.8 M sulfuric acid at 16 V, K is equal to 1.18. Therefore, we can suggest that the mechanism of pore formation at the initial stage of oxide growth is the same for different U_a values and electrolyte types.

To explain the development mechanism of minor pores at the initial stage of anodic film growth, we assumed that such pores develop only inside hexagonal elemental cells composed of the major pores as a result of an energetically more efficient mechanism. In this case, the basis for forming a smaller hexagonal cell consisting of such pores is the major pore in the center with smaller pores at the tops located in the middle of the faces of the main cell. Fig. 4 shows a model for the simultaneous development of major and minor pores based on an elementary hexagonal cell composed of major pores.

Based on a geometric model with the arrangement of pores of a smaller diameter inside an elementary hexagonal cell with major pores in the center and at the tops, it was found that the ratio of interpore distances for such groups of pores is equal to $2/\sqrt{3}$. Therefore, K is also equal to $2/\sqrt{3}$. This agrees with the experimental data presented in Table 1. Minor deviations of the experimental ratios from the calculated ratio can be explained by the shape distortion of the real porous cells from the ideal hexagonal shape.

The presented model shows that the development of minor pores stops when the anodic film reaches a thickness of about 2–3 diameters of the interpore distance. The reason for this phenomenon is a rapid increase in the compressive mechanical stresses in aluminum oxide with an increase in the thickness of the cells due to the growth of porous anodic alumina film [20,21]. According to the evaluation, the thickness of the layer with disordered pores for porous anodic alumina film formed at 40 V in oxalic acid is about 200–300 nm, which agrees with data in [22–24].

Of great interest is the study and analysis of the surface morphology of porous anodic alumina for an array of pores containing major and minor pores.

In Fig. 5, one can see individual pores (marked in blue) with a diameter smaller than the major pores in places close to the middle of the faces of the elementary hexagonal cells formed by the major pores (marked in red). However, it should be noted that the real porous structure of anodic films can differ significantly from their ideal structure. Considering this, the observed pore deviations of a smaller diameter from the locations predicted by the theory might be a consequence of the elemental cell deviation, composed of the major pores, from their ideal hexagonal shape.

It should also be highlighted that the regularities in the simultaneous formation of the major and minor pores at the initial stage of aluminum anodization agree with the pore branching effect, i.e., the possibility of dividing one pore into several pores with a decrease in voltage during the anodizing process [1,25,26]. As was shown in [27,28], the

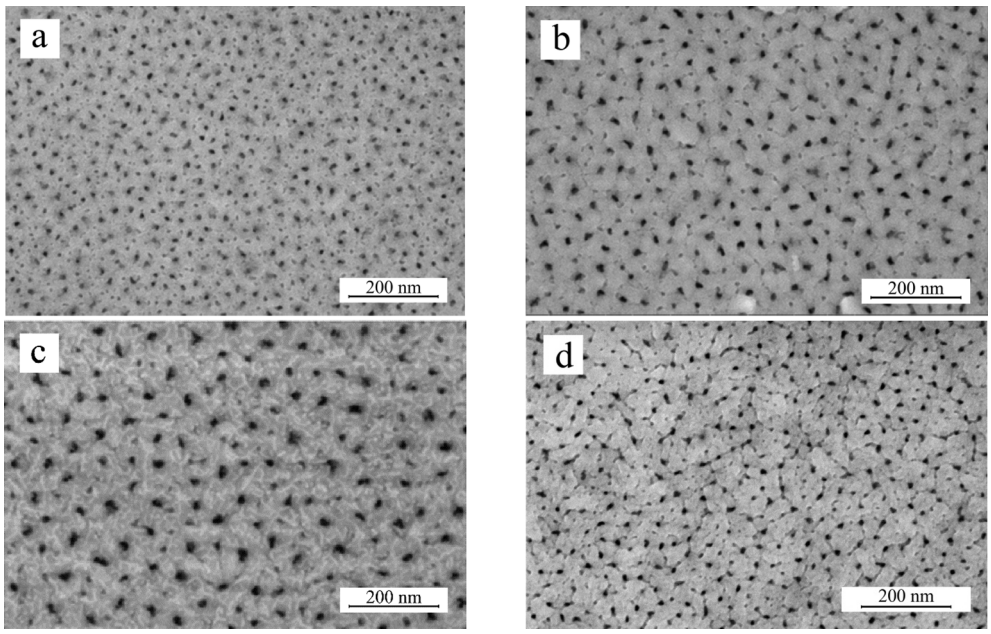

Fig. 2. SEM images of the surface morphology of porous alumina films on SiO_2/Si substrates obtained in oxalic acid at U_a values of (a) 10 V, (b) 20 V, (c) 30 V, and (d) in sulfuric acid at 16 V.

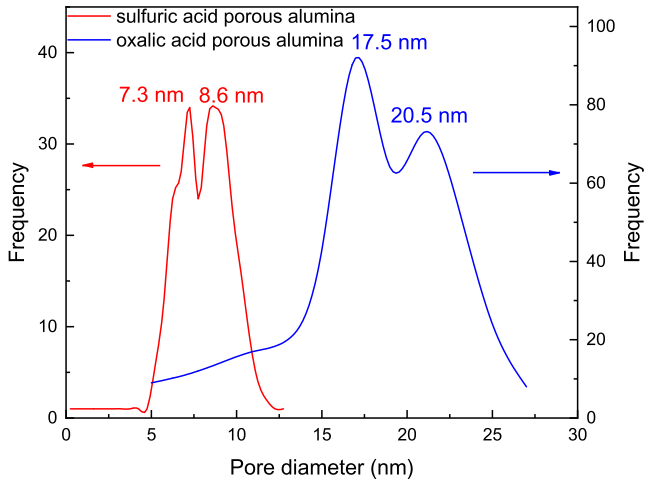

Fig. 3. Pore diameter distributions for porous anodic alumina films formed on a SiO_2/Si substrate in 0.3 M oxalic acid at 30 V and 1.8 M sulfuric acid at 16 V.

Table 1
Diameters of the major and minor pores and their ratios for films of porous anodic alumina on SiO_2/Si substrates obtained at 10–50 V in 0.3 M oxalic acid.

U_a, V	10	15	20	30	40	50
D, nm	12.2 ± 0.2	14.4 ± 0.3	15.6 ± 0.5	20.5 ± 0.7	26.5 ± 0.7	31.7 ± 0.7
d, nm	10.5 ± 0.3	12.5 ± 0.4	13.3 ± 0.4	17.5 ± 0.6	22.4 ± 0.7	26.8 ± 0.7
K	1.16	1.15	1.17	1.17	1.18	1.18

branching of one pore into two parts only occurs when the U_a decreases by $\sqrt{2}$ times. The model of pore branching with decreasing voltage, as in our case, is based on an energy-efficient mechanism for the rearrangement of the porous structure. Following this model, the area of two new hexagonal cells with pores in the center and at the tops should coincide with the area of one primary hexagonal cell. From geometric considerations, it follows that when the interpore distance differs by $\sqrt{2}$ times from the initial value (correspondingly, the voltage value decreases by $\sqrt{2}$ times compared to the initial voltage), then the mechanism for commencing the division of one pore into two will be initiated. Based on the pore branching laws [29], various approaches were proposed for manufacturing porous anodic alumina asymmetric matrices.

As seen in Fig. 6, the pore distribution by diameter has only one maximum at 39.4 nm, indicating the formation of a highly ordered porous structure at the initial stage of aluminum anodization. The insert shows that the porous film has a highly ordered structure with hexagonal pore arrays.

Therefore, at the initial stage of disordered porous anodic film growth for the aluminum anodizing process, only two large groups of pores receive dominant development from all centers of pore nucleation: the major and minor pores, the diameters of which are $2/\sqrt{3}$ times smaller than the major pores. The development of smaller pores (in size) is not random; it occurs in compliance with the possibility of pore development inside the hexagonal cells formed from the major pores.

4. Conclusions

It was demonstrated that a characteristic feature of disordered porous anodic film growth at the initial stage of the aluminum anodizing process is the simultaneous development of two large groups of pores: major pores and minor pores. For anodizing voltages in the range 10–50 V in oxalic acid, the ratio of the diameters of such pores was approximately 1.17 or $2/\sqrt{3}$. It was assumed that a group of identical pores with a smaller diameter than the diameter of the major pores could develop only at specific points inside the elementary hexagonal cells composed of the major pores as a result of an energetically more efficient mechanism. Moreover, the basis for forming a smaller hexagonal cell consisting of such pores is the major pore in the center and smaller pores at the tops located in the middle of the faces of the main cell.

It can be concluded that the development of an equal pore group with a smaller diameter is blocked when the anode film reaches a thickness of about 2–3 diameters of the interpore distance. The reason for this phenomenon is the increase in compressive mechanical stresses in aluminum oxide with an increased thickness of the anodic film.

It was shown that the development of minor pores instead of major pores at the initial stage of the disordered porous anodic film growth is

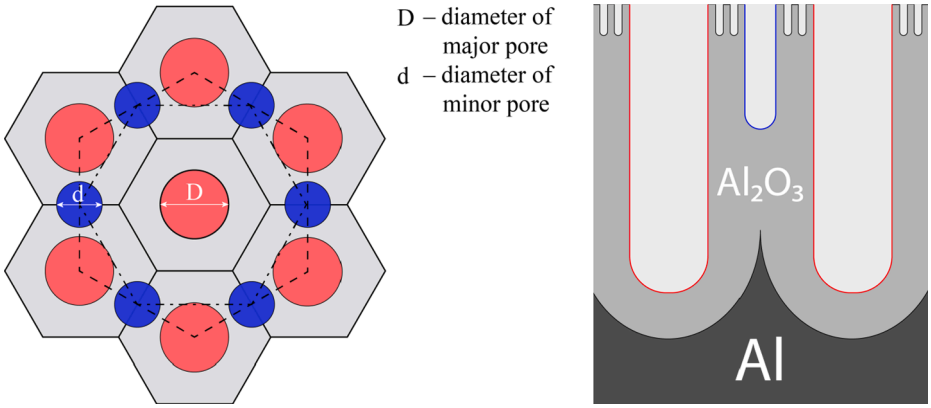

Fig. 4. Model for the simultaneous development of the major and minor pores inside an elementary hexagonal cell composed of the major pores.

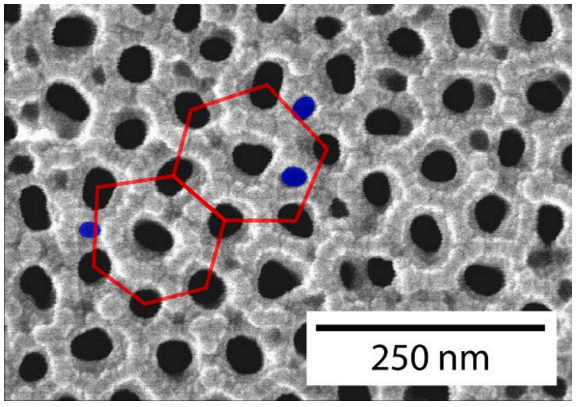

Fig. 5. SEM image of the surface morphology of a porous anodic alumina film formed in 0.3 M oxalic acid (40 V, 20 °C) on aluminum foil after electrochemical polishing.

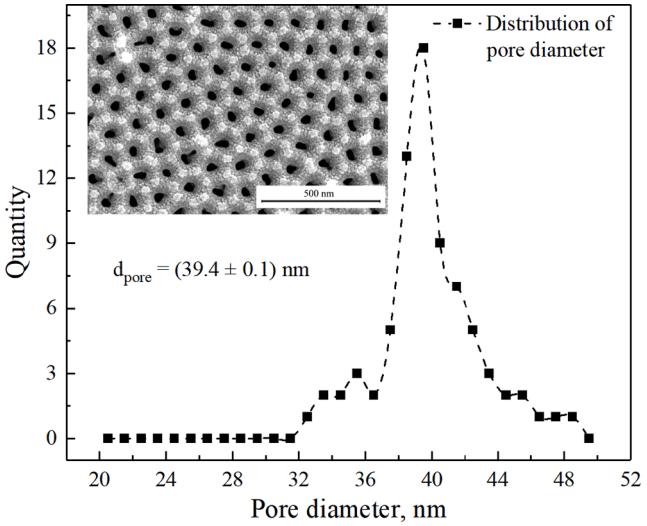

Fig. 6. Pore distribution by diameter for a porous anodic alumina film formed on aluminum foil by two-stage anodization in oxalic acid at 50 V. Inset is a SEM image of the surface morphology of a porous anodic alumina film obtained in this mode.

not random. Rather, it is determined by the energy-efficient conditions for developing pores inside hexagonal cells formed from the major pores broken due to the growth of compressive mechanical stresses.

Formatting of funding sources

This work was supported by the Belarusian Republican Foundation for Fundamental Research [Grant No B22KI-044].

CRediT authorship contribution statement

Katsiaryna Chernyakova: Formal analysis, Investigation, Visualization, Writing – original draft, Writing – review & editing. **Vaclovas Klimas:** Investigation, Resources, Visualization, Validation. **Arunas Jagminas:** Conceptualization, Supervision, Resources, Writing – review & editing. **Nikita Lushpa:** Investigation, Visualization, Validation. **Igor Vrublevsky:** Conceptualization, Resources, Methodology, Supervision. **Sigitas Jankauskas:** .

Declaration of Competing Interest

The authors declare that they have no known competing financial interests or personal relationships that could have appeared to influence the work reported in this paper.

Data availability

No data was used for the research described in the article.

References

[1] A. Ruiz-Clavijo, O. Caballero-Calero, M. Martín-González, Nanoscale 13 (2021) 2227–2265, https://doi.org/10.1039/D0NR07582E.
[2] J.T. Domagalski, E. Xifre-Perez, L.F. Marsal, Nanomaterials 11 (2021) 430, https://doi.org/10.3390/nano11020430.
[3] A. Santos, T. Kumeria, D. Losic, Materials 7 (2014) 4297–4320, https://doi.org/10.3390/ma7064297.
[4] W. Lee, S.-J. Park, Chem. Rev. 114 (2014) 7487–7556, https://doi.org/10.3390/ma7064297.
[5] C.T. Sousa, D.C. Leitao, M.P. Proenca, J. Ventura, A.M. Pereira, J.P. Araujo, Appl. Phys. Rev. 1 (2014), 031102, https://doi.org/10.1063/1.4893546.
[6] H. Masuda, K. Fukuda, Science 268 (1995) 1466–1468, https://doi.org/10.1126/science.268.5216.1466.
[7] H. Masuda, H. Yamada, M. Satoh, H. Asoh, M. Nakao, T. Tamamura, Appl. Phys. Lett. 71 (1997) 2770–2772, https://doi.org/10.1063/1.120128.
[8] S.J. Garcia-Vergara, P. Skeldon, G.E. Thompson, H.A. Habazaki, Electrochim. Acta 52 (2006) 681–687, https://doi.org/10.1016/j.electacta.2006.05.054.
[9] J.E. Houser, K.R. Hebert, Nat. Mater. 8 (2009) 415–420, https://doi.org/10.1038/nmat2423.
[10] K. Chernyakova, B. Tzaneva, I. Vrublevsky, V. Videkov, J. Electrochem. Soc. 167 (2020), 103506, https://doi.org/10.1149/1945-7111/ab9d65.
[11] L. Zaraska, W.J. Stepniowski, E. Ciepiela, G.D. Sulka, Thin Solid Films 534 (2013) 155–161, https://doi.org/10.1016/j.tsf.2013.02.056.
[12] K. Chernyakova, I. Vrublevsky, V. Klimas, A. Jagminas, J. Electrochem. Soc. 165 (2018) E289–E293, https://doi.org/10.1149/2.1001807jes.
[13] D. Nakajima, T. Kikuchi, S. Natsui, R.O. Suzuki, Appl. Surf. Sci. 321 (2014) 364–370, https://doi.org/10.1016/j.apsusc.2014.10.014.
[14] S. Stojadinovic, R. Vasilic, I. Belca, M. Tadic, B. Kasalica, L. Zekovic, Appl. Surf. Sci. 255 (2008) 2845–2850, https://doi.org/10.1016/j.apsusc.2008.08.023.

[15] K. Chernyakova, R. Karpicz, S. Zavadski, O. Poklonskaya, A. Jagminas, I. Vrublevsky, J. Lumin. 182 (2017) 233–239, https://doi.org/10.1016/j.jlumin.2016.10.026.
[16] D. Nakajima, T. Kikuchi, T. Yoshioka, H. Matsushima, M. Ueda, R.O. Suzuki, S. Natsui, Materials 12 (2019) 3497, https://doi.org/10.3390/ma12213497.
[17] K. Chernyakova, R. Karpicz, D. Rutkauskas, I. Vrublevsky, A.W. Hassel, Physica Status Solidi (a) 215 (2018) 1700892, https://doi.org/10.1002/pssa.201700892.
[18] W.J. Stępniowski, M. Michalska-Domańska, M. Norek, E. Twardosz, W. Florkiewicz, W. Polkowski, D. Zasada, Z. Bojar, Surf. Coat. Technol. 258 (2014) 268–274, https://doi.org/10.1016/j.surfcoat.2014.09.013.
[19] F. Le Coz, L. Arurault, L. Datas, Mater. Charact. 61 (2010) 283–288, https://doi.org/10.1016/j.matchar.2009.12.008.
[20] Ö.Ö. Çapraz, P. Shrotriya, P. Skeldon, G.E. Thompson, K.R. Hebert, Electrochim. Acta 159 (2015) 16–22, https://doi.org/10.1016/j.electacta.2015.01.183.
[21] K. Chernyakova, I. Vrublevsky, A. Jagminas, V. Klimas, J. Solid State Electr. 25 (2021) 1453–1460, https://doi.org/10.1007/s10008-021-04925-x.
[22] Z. Ling, Y. Li, in: D. Losic, A. Santos (Eds.), Nanoporous Alumina, Springer Ser Mater Sci S219, Springer Int. Publishing AG Switzerland, 2015, pp. 1–30. https://doi.org/10.1007/978-3-319-20334-8_1.
[23] M. Iwai, T. Kikuchi, R.O. Suzuki, ECS J. Solid State Sci. Technol. 9 (2020), 044004, https://doi.org/10.1149/2162-8777/ab89ba.
[24] A. Baron-Wiecheć, J.J. Ganem, S.J. Garcia-Vergara, P. Skeldon, G.E. Thompson, I. C. Vickridge, J. Electrochem. Soc. 157 (2010) C399–C407. doi:10.1149/1.3490640. 10.1149/1.3490640.
[25] S.S. Chen, Z.Y. Ling, X. Hu, Y. Li, J. Mater. Chem. 19 (2009) 5717–5719, https://doi.org/10.1039/B908815F.
[26] D.I. Petukhov, K.S. Napolskii, A.A. Eliseev, Nanotechnology 22 (2012), 335601, https://doi.org/10.1088/0957-4484/23/33/335601.
[27] C. Papadopoulos, A. Rakitin, J. Li, A.S. Vedeneev, J.M. Xu, Phys. Rev. Lett. 85 (2000) 3476–3479, https://doi.org/10.1103/physrevlett.85.3476.
[28] J. Li, C. Papadopoulos, J. Xu, Nature 402 (1999) 253–254, https://doi.org/10.1038/46214.
[29] T. Inada, N. Uno, T. Kato, Y. Iwamoto, J. Mater. Res. 20 (2005) 114–120, https://doi.org/10.1557/JMR.2005.0016.